AIAA JOURNAL
Vol. 32, No. 9, September 1994

Validation Procedure for the Analysis of Shock-Wave/Boundary-Layer Interaction Problems

F. Grasso*
University of Rome "La Sapienza," 00184 Rome, Italy
G. Leone†
CIRA, 81043 Capua (CE), Italy
and
J. M. Delery‡
ONERA, 92320 Chatillon, France

The present work deals with the validation of hypersonic flow simulation in the presence of strong shock-wave/boundary-layer interaction phenomena. In particular, we have discussed the meaning of validation from a numerical and experimental point of view and have shown the consistency requirements that must always be satisfied when performing a numerical simulation. The equations solved are the Reynolds-averaged Navier-Stokes equations with an algebraic turbulence model. The method employs a Runge-Kutta finite-volume formulation with symmetric discretization of both inviscid and viscous fluxes. The technique has been applied to analyze shock-wave/boundary-layer interactions and their effects on heating rates, peak heating location, and separation extent.

I. Introduction

THE development of high-speed maneuverable re-entry vehicles has refocused attention on the problem of accurately predicting shock-wave/boundary-layer interaction phenomena. The latter are often present in regions such as control surfaces, intakes, etc., and the correct estimates of pressure distribution, heat loads, etc. is a crucial matter for the design of high-speed vehicles. Indeed, in hypersonic flows the shock-wave/boundary-layer interaction often produces flow separation, a subsequent reattachment (either laminar or turbulent, depending on the flight conditions), a recirculation bubble with a consequent loss in aerodynamic performance, etc.

In the present work we have studied the flow over compression ramps and have addressed the problem of developing a validation procedure for analyzing viscous-inviscid interaction phenomena. This aspect of validation is receiving considerable attention due to its importance in the development of computational fluid dynamics tools.[1,5] As pointed out by both Marvin[1] and Bogdonoff,[5] validation involves both numerical and physical aspects. The former requires the assessment of the sensitivity of the solution to the numerical algorithm, grid resolution, and its geometry. Moreover, to address the numerical aspects of validation the sensitivity of the solutions to the parameters that affect the accuracy of the scheme must be investigated for an estimate of the error magnitude.

The physical aspect of validation implies that the experimental and theoretical knowledge of the phenomena must be taken into account when analyzing the computational solution. In particular, in simulating shock-wave/boundary-layer interaction problems one should always pose the question as to whether or not the computed solution is physically correct. To answer such a question one must guarantee that the computed results satisfy consistency constraints that have to come from theoretical and/or experimental knowledge. For example, for the problem we have investigated a few fundamental aspects are well-established (and should be recovered by any computed solution): 1) in the near leading edge region, if one neglects high Knudsen number effects, the solution is affected by the (strong) viscous interaction; 2) along the leading edge flat plate the behavior of the solution should recover a boundary-layer-type solution up to the extent of the upstream influence; 3) in the region where the interaction takes place the computed results should be consistent with well-established experimental correlations; and 4) along the ramp the behavior of the flow, past the reattachment if separation arises, can be characterized by the inviscid pressure jump.

In the present work we have developed a validation procedure in light of the preceding considerations and have analyzed flows over compression ramps (both from the experimental and numerical point of view) for a variety of flow conditions differing in Mach and Reynolds numbers, ramp angles, geometry, etc.

In the next section the numerical and experimental procedures, as well as the validation approach and some applications, will be described.

II. Numerical Procedure

The governing equations are the two-dimensional, Reynolds-averaged Navier-Stokes equations. In vector form one has

$$\frac{\partial}{\partial t}\int_V \boldsymbol{W}\,\mathrm{d}v + \int_S [(\boldsymbol{F}_E - \boldsymbol{F}_V)\cdot \boldsymbol{n}]\,\mathrm{d}S = 0 \tag{1}$$

The vector unknown $\boldsymbol{W}$, the inviscid ($\boldsymbol{F}_E$) and the viscous ($\boldsymbol{F}_V$) fluxes are defined as

$$\boldsymbol{W} = \begin{bmatrix} \rho \\ \rho u \\ \rho v \\ \rho E \end{bmatrix} \quad \boldsymbol{F}_E^x = \begin{bmatrix} \rho u \\ \rho u^2 + p \\ \rho uv \\ \rho uH \end{bmatrix} \quad \boldsymbol{F}_E^y = \begin{bmatrix} \rho v \\ \rho uv \\ \rho v^2 + p \\ \rho vH \end{bmatrix}$$

$$\boldsymbol{F}_V^x = \begin{bmatrix} 0 \\ \sigma_x \\ \tau_{xy} \\ u\sigma_x + v\tau_{xy} - Q_x \end{bmatrix} \quad \boldsymbol{F}_V^y = \begin{bmatrix} 0 \\ \tau_{xy} \\ \sigma_y \\ u\tau_{xy} + v\sigma_y - Q_y \end{bmatrix}$$

Received May 20, 1993; revision received Nov. 5, 1993; accepted for publication Dec. 4, 1993.

*Professor, Department of Mechanics and Aeronautics, via Eudossian 18.
†Senior Researcher, Aerothermodynamic Section, via Maiorise.
‡Head, Aerodynamic Division.

where

$$\sigma = \mu[\text{grad}\boldsymbol{v} + (\text{grad}\boldsymbol{v})^T] - \frac{2}{3}\mu(\text{div}\boldsymbol{v})\boldsymbol{I}$$

$$\boldsymbol{Q} = -\lambda \text{grad}T$$

$$E = e + \frac{u^2 + v^2}{2}$$

$$h = e + \frac{p}{\rho}$$

$$H = E + \frac{p}{\rho}$$

$$p = \rho RT$$

and h, e, and R are, respectively, the enthalpy and the gas constant, and $\boldsymbol{I}$ is the unit tensor. The laminar viscosity is defined by Sutherland's law:

$$\frac{\mu}{\mu_{\text{ref}}} = \frac{T}{T_{\text{ref}}}\frac{T_{\text{ref}} + S}{T + S}$$

with $T_{\text{ref}} = 288$ K, $\mu_{\text{ref}} = 1.789 \times 10^{-5}$, and $S = 110$ K.

The main objective of the present work is not development of a turbulence model, but the validation aspects of a hypersonic flow simulation. As a consequence, to account for turbulence, an algebraic model has been employed. In particular, the turbulent viscosity is derived using a Baldwin-Lomax turbulence model,[8] and the heat conduction coefficient is computed using the Prandtl number definition.

The equations are discretized by using a cell-centered finite-volume formulation with symmetric discretization of both the inviscid and viscous terms. Approximating surface and boundary integrals by means of the mean value theorem and midpoint rule, the following system of ordinary differential equations is obtained for each computational cell[6,7]:

$$S_{i,j}\frac{d\boldsymbol{W}_{i,j}}{dt} + \sum_{\beta=1}^{4}(\boldsymbol{F}_{\text{num}} \cdot \boldsymbol{n}\Delta s)_\beta = 0$$

where β stands for the generic cell face, $\boldsymbol{n}$ is the positive unit normal to the cell face whose length is Δs, $S_{i,j}$ is the cell area, and $\boldsymbol{F}_{\text{num}}$ is the numerical flux vector.

The numerical algorithm employs a symmetric discretization of both the inviscid and viscous terms, and time integration is performed by a five-stage Runge-Kutta scheme:

$$\begin{aligned} \boldsymbol{W}_{i,j}^{(0)} &= \boldsymbol{W}_{i,j}^{n} \\ \boldsymbol{W}_{i,j}^{(k)} &= \boldsymbol{W}_{i,j}^{(0)} - \alpha_k \frac{\Delta t_{i,j}}{S_{i,j}}(\boldsymbol{R}_I^{(k-1)} + \boldsymbol{R}_V^{(0)} - \boldsymbol{R}_{AD}^{(k)})_{i,j} \\ \boldsymbol{W}_{i,j}^{(n+1)} &= \boldsymbol{W}_{i,j}^{(5)} \end{aligned} \qquad (2)$$

where $\boldsymbol{R}$ represents the inviscid ($\boldsymbol{R}_I$), viscous ($\boldsymbol{R}_V$), and dissipation ($\boldsymbol{R}_{AD}$) contributions. The coefficients of the Runge-Kutta scheme are set equal to

$$\alpha_1 = 0.25, \quad \alpha_2 = 0.166, \quad \alpha_3 = 0.375, \quad \alpha_4 = 0.50, \quad \alpha_5 = 1.0$$

The numerical inviscid flux contribution is evaluated by means of a consistent conservative cell-centered formulation which yields:

$$\boldsymbol{R}_I(\boldsymbol{W}_{i,j}) = \sum_{\beta=1,4}(\boldsymbol{F}_{E,\text{num}} \cdot \boldsymbol{n})_\beta \Delta s_\beta$$

where β indicates the cell faces and the subscript num stands for numerical. $\boldsymbol{F}_{E,\text{num}}$ at the midpoint of cell face $(i+1/2, j)$ is:

$$(\boldsymbol{F}_{E,\text{num}} \cdot \boldsymbol{n})_{i+1/2,j} = 1/2\,(\boldsymbol{F}_{E_{i,j}} + \boldsymbol{F}_{E_{i+1,j}}) \cdot \boldsymbol{n}_{i+1/2,j}$$

The numerical viscous flux contribution is cast in the following form

$$\boldsymbol{R}_V(\boldsymbol{W}_{i,j}) = \sum_{\beta=1,4}(\boldsymbol{F}_{V,\text{num}} \cdot \boldsymbol{n})_\beta \Delta s_\beta$$

where the discretized viscous flux contribution at cell face $(i + 1/2, j)$ is obtained by means of the Gauss theorem.

Adaptive dissipation is usually added for inviscid flow computations to prevent oscillations and even/odd point decoupling.[6] Viscous high-speed flows are generally characterized by very steep gradients that may enhance the nonlinear effects. Consequently, the physical dissipation may not be sufficient to dampen the oscillations, and adaptive dissipation is still added.[7] The latter contribution is defined as:

$$\boldsymbol{R}_{AD}(\boldsymbol{W}_{i,j}) = \sum_{\beta=1,4}(\boldsymbol{F}_{AD} \cdot \boldsymbol{n})_\beta \Delta s_\beta$$

The adaptive dissipation flux $\boldsymbol{F}_{AD}$ at cell face $(i+1/2, j)$ is:

$$\begin{aligned} &(\boldsymbol{F}_{AD} \cdot \boldsymbol{n}\Delta s)_{i+1/2,j} \\ &= \lambda_{i+1/2,j}(\varepsilon^{(2)}_{i+1/2,j}\Delta_i^+ \boldsymbol{W}_{i,j} - \varepsilon^{(4)}_{i+1/2,j}\Delta_i^+\Delta_i^-\Delta_i^+\boldsymbol{W}_{i,j}) \end{aligned}$$

where Δ_i^+ and Δ_i^- represent, respectively, the forward and backward difference operators in the logical i-direction. The variables $\lambda_{i+1/2,j}$, $\varepsilon^{(2)}_{i+1/2,j}$, and $\varepsilon^{(4)}_{i+1/2,j}$ are, respectively, the spectral radius of the inviscid flux Jacobian, and the second- and fourth-order pressure sensors, defined as:

$$\varepsilon^{(2)}_{i+1/2,j} = k^{(2)}\max(\nu_{i-1,j}, \nu_{i,j}, \nu_{i+1,j}, \nu_{i+2,j})$$

$$\varepsilon^{(4)}_{i+1/2,j} = \max[0, (k^{(4)} - \varepsilon^{(2)}_{i+1/2,j})]$$

In the present work the classical shock sensor definition (ν) has been used rather than the one recently developed by Swanson and Turkel.[9]

III. Validation Procedure

To develop a validation procedure for analyzing viscous-inviscid interaction phenomena, both the numerical and physical aspects of validation have to be addressed. In particular, the numerical aspect amounts to assess the sensitivity of the solutions to the numerical algorithm, grid resolution, and its geometry, as well as the sensitivity to the parameters that affect the accuracy of the scheme. This aspect has been investigated in detail and the methodology followed is described in the application section.

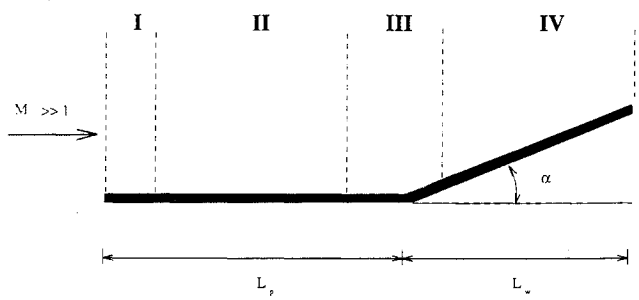

Fig. 1 Ramp flow.

The physical aspect of validation requires a careful analysis to guarantee that the computed solution is consistent with experimentally measured data, as well as theoretically well-established behaviors. Moreover, the flow conditions have to be carefully analyzed a priori for a proper modeling (i.e., laminar, turbulent, transitional, nonequilibrium effects, etc.).

In particular, in simulating flows over compression ramps (characterized by shock-wave/boundary-layer interactions) one can identify different regions.

In the near leading edge region (region I of Fig. 1), neglecting high Knudsen number effects, the flow is dominated by strong viscous interactions. As a consequence, the pressure, the skin friction, and the Stanton number distribution depend strongly on the viscous interaction parameter $\bar{\chi}$ and should compare well with the viscous interaction results. For example, for the test case analyzed herein, the pressure can be estimated by the formula:

$$\frac{p}{p_\infty} = 1 + A\bar{\chi} \tag{3}$$

where $\bar{\chi} = (M^3/\sqrt{Re})\sqrt{(\rho_w\mu_w)/(\rho_\infty\mu_\infty)}$, and A depends on $\bar{\chi}$ and the wall temperature.

The preceding formula is of great usefulness. Indeed, it can be used to assess the quality of the near leading edge grid to obtain an accurate resolution of the leading edge shock and its interaction with the boundary layer.

Along the leading edge flat plate and up to the interaction (region II), the behavior of the flow is of a boundary-layer type, and the Eckert reference enthalpy method can be employed to evaluate the high Mach number effects on the skin friction (c_f) and Stanton number (St) yielding:

$$c_f = KRe_x^{-n}\left(\frac{T^*}{T_\infty}\right)^{-n(1-\omega)}\left(\frac{p}{p_\infty}\right)^n \tag{4}$$

$$St = 1/2\, Pr^{-2/3} c_f \tag{5}$$

where $K = 0.664$ and $n = 0.5$ for laminar conditions, and $K = 0.0583$ and $n = 0.2$ for turbulent conditions, and $\omega \simeq 3/4$ is the exponent of the viscosity law. Observe that Eqs. (3–5) show that the skin friction and Stanton number are affected both by the Mach number (through the temperature dependency) and the viscous interaction parameter. The reference temperature T^* (a given temperature within the boundary layer) can be evaluated by means of the following formula[10]:

$$\frac{T^*}{T_e} = 1. + 0.032\, M_e^2 + 0.58\left(\frac{T_w}{T_e} - 1\right) \tag{6}$$

In the region where the interaction takes place (region III of Fig. 1) the computed results should be consistent with the results of the free interaction theory as described in Refs. 11 and 15. Accordingly, the separation can be characterized by the conditions of the flow immediately upstream of the interaction, i.e.,

$$\frac{p - p_0}{q_0} = (2c_{f_0})^{1/2}\,(M_0^2 - 1)^{-1/4}\, F\left(\frac{X - X_0}{L}\right) \tag{7}$$

where the subscript 0 indicates the conditions upstream of the interaction. F is a function that correlates the pressure rise to the distance measured with respect to the beginning of the interaction (normalized by the distance L from the origin of the interaction where the pressure reaches a plateau).

Equation (7) can be used to obtain the values of the plateau and the separation pressures for both laminar and turbulent flow conditions. Indeed, at separation, F is equal to 0.79 and 4.2, respectively, for laminar and turbulent conditions, while in the recirculation region F is equal to 1.46 and 6, respectively, for laminar and turbulent plateau values.

Another parameter that characterizes the presence of separation is the incipient separation angle that is defined as the (ramp) angle at which the flow first separates. Such an angle can be correlated to the Mach number and the interaction parameter $\bar{\chi}$ (Refs. 11 and 12)

$$\frac{\theta_{is}}{\sqrt{M_\infty}} = \alpha\left(\frac{c^*}{Re_{x0}}\right)^\beta \tag{8}$$

where $C^* = (\rho_w\mu_w)/(\rho_\infty\mu_\infty)$ and Re_{x0} is the Reynolds number, using the interaction location as reference length. The experimentally determined values of α and β are, respectively, 80 and 0.25 for laminar flows, and 42 and 0.086 for turbulent flows.

Along the ramp (region IV of Fig. 1) the flow is mainly characterized by the (strong) shock wave that arises at the wedge hinge, and the peak heating correlates well with the inviscid pressure jump as suggested by Hung and Barnett.[14] For fully laminar flows (corresponding to $Re_L < 5 \times 10^5$) we have:

$$\frac{\dot{q}_{pk}}{\dot{q}_{\text{ref}}} = 0.13\left(\frac{p_3}{p_1}\right)^{1.13} \tag{9}$$

and for transitional or turbulent flows:

$$\frac{\dot{q}_{pk}}{\dot{q}_{\text{ref}}} = 0.468(Re_l \times 10^{-6})^{1.85} \cdot \left(\frac{p_3}{p_1}\right)^{1.13} \tag{10}$$

The use of the preceding formula requires knowledge of the reference heating. Numerical experiments performed by two of the present authors[16] have shown that such a quantity can be defined by means of Eckert's formula, evaluated at the location immediately before the location where the interaction takes place, yielding:

$$\dot{q}_{\text{ref}} = \tilde{St} \cdot \left(1 + Pr^\alpha \frac{\gamma - 1}{2} M_\infty^2 - \frac{T_w}{T_\infty}\right)\rho_e u_e h_\infty \tag{11}$$

where $\tilde{St}$ is a reference Stanton number evaluated by means of Eq. (5), and $\alpha = 1/2$ for laminar flows, and $\alpha = 1/3$ for turbulent flows.

In the presence of a laminar-turbulent transition, a critical point is the evaluation of the transition location. Experimental correlations, mainly extrapolated from lower Mach number regimes and based on the analysis of the boundary layer characteristics, can be used to evaluate the transition onset. In particular, in the present work the transition location has been estimated by extending an experimentally developed criteria for hypersonic boundary layer transitions on sharp cones.[13]

$$\log_{10}(Re_t) = 6.421 \exp[1.209 \times 10^{-4}\, M_e^{2.641}] \tag{12}$$

Moreover, it must be pointed out that the preceding formula accounts for neither the properties of the boundary layer, nor for the viscous interaction effects. Therefore, a different correlation formula, derived from flight data, that gives the transition position as a function of the Mach number and the Reynolds number, based on the momentum thickness (θ_t), has been used:

$$\frac{Re_{\theta_t}}{M_e} \le K(M_e, Re_e, \bar{\chi}, \cdots) \tag{13}$$

where $Re_{\theta_t} = (\rho_e U_e \theta_t)/\mu_e$ and $K = \mathcal{O}(100 \div 200)$, and the momentum thickness can be evaluated from Eckert's reference temperature method.

IV. Applications

The flow over compression ramps has been analyzed, and the geometry and the conditions of the different test cases are given in Table 1.

Table 1 Geometry and test cases conditions

Test case	A	B.1	B.2
M_∞	10	10	10
Re_∞/m	9×10^6	1.68×10^5	1.68×10^5
T_∞, K	50	52.5	52.5
T_{wall}, K	288	290	290
L_p, cm	25	17.9	17.9
L_w, cm	10	7.1	9
α_w, deg	15	15	25

Table 2 Characteristics of the grids used for test case A

Grid	Mod.	Xtr	*AR*	Dy_{min}/L_p
1	L	—	1.6:26.8	0.790E-4
2	L/T	0.02	1.9:52.2	0.400E-4
3	L/T	0.02	3.0:229	0.920E-5
4	L/T	0.02	3.4:155	1.30E-5
5	L/T	0.02	2.1:333	0.630E-5
6	L/T	0.02	1.5:782	0.270E-5
7	T	0.02	1.2:1962	0.110E-5
8	L/T	0.02	1.5:782	0.135E-5

Test Case A: Transitional Flow

For this test case the model consisted of a flat plate, with a sharp leading edge set at zero incidence in a supersonic uniform flow of Mach number 10. This plate, with a span equal to 200 mm, was equipped with a ramp of angle $\alpha = 15$ deg. The model had a total length of 347 mm, with the distance L_p between the leading edge and the ramp hinge line being equal to 250 mm. The tests have been executed in the hypersonic blow-down facility of the ONERA Chalais-Meudon Establishment, with a stagnation pressure of 125×10^5 Pa and a stagnation temperature of 1100 K, leading to a unit Reynolds number close to 9×10^6/m. In the present experiments, the wall of the model was at ambient temperature ($T_w = 288$ K) and the surface measurements were performed in the model plane of symmetry. The pressure distribution was determined by means of PSI-type transducers placed as close to the orifices as possible to minimize the response time, thus allowing a correct stabilization of the transducers' indication. The heat transfer distribution was determined by the thick wall calorimetric method with Chromel-Arcal-type thermocouples.[17] The Reynolds number level of this experiment was such that the first part of the separation induced by the ramp was laminar, as demonstrated by Schlieren photographs and the behavior of the wall heat transfer. However, the amplitude of the heat transfer peak at the reattachment tends to prove that transition began somewhere between separation and reattachment, taking into consideration the correlation of Hung and Barnett.[14]

This test case, corresponding to case III.3 of the Hermes Workshop,[3] has been analyzed to assess the influence of the grid sensitivity and to show the importance of a correct modeling of the problem.

Several computations have been performed, differing in the total number of cells. In particular, a 176×64 and a 352×128 points mesh were selected for analyzing both the effects of grid refinement and the influence of stretching and aspect ratio distribution for a given grid. The assessment of the grid properties on the solution is useful when limited computing resources are available so as to minimize the number of cells needed to obtain solutions as accurate as possible. The characteristics of the grids are given in Table 2, in which the minimum mesh spacing in the normal direction, the nondimensional transition location, the aspect ratios, and the modeling (i.e. laminar or turbulent flow) are specified. The computed pressure coefficient and Stanton number distribution obtained using the grids labeled 6 and 8 in Table 2 are reported in Figs. 2 and 3. For a given aspect ratio distribution, doubling the number of the mesh points in the two directions affected mainly the extent of the recirculation region and separation shock location. The peak values of the pressure and heating rates were rather insensitive. Computations were also performed on a grid with 88×32 points (not reported here) yielding a dramatic change in the flow characteristics: no separation in the flow was observed. The influence of the total number of mesh points (N_p) is summarized in Fig. 4, which shows the separation and reattachment shock locations, and the peak values of pressure and Stanton number vs $1/N$.

Figures 5 and 6 compare of the computed pressure and Stanton number distributions along the wall with the experimental values, with the assumption of fully laminar flow. An increase in the as-

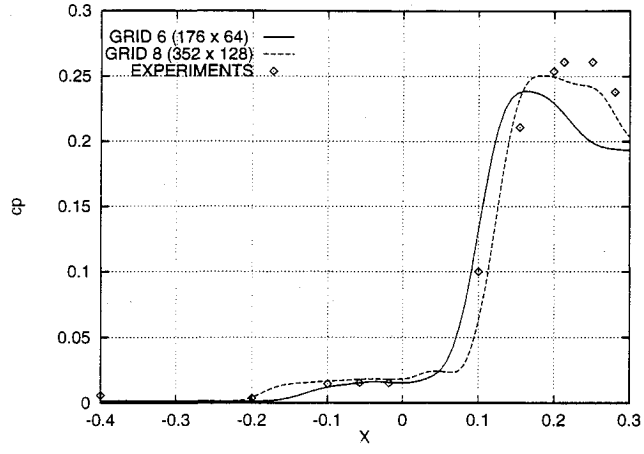

Fig. 2 Test case A: pressure coefficient.

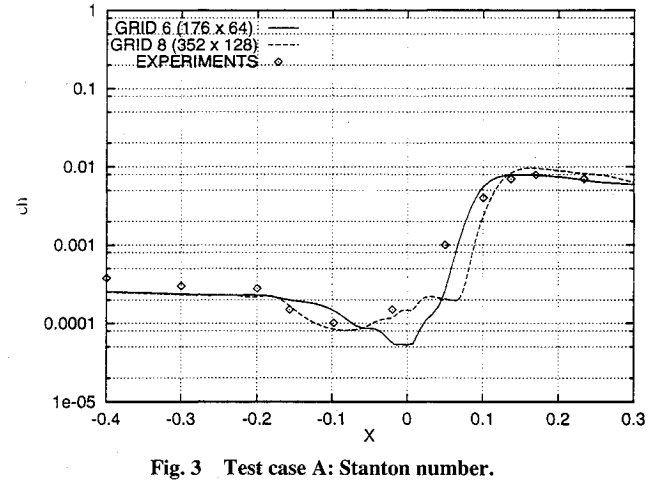

Fig. 3 Test case A: Stanton number.

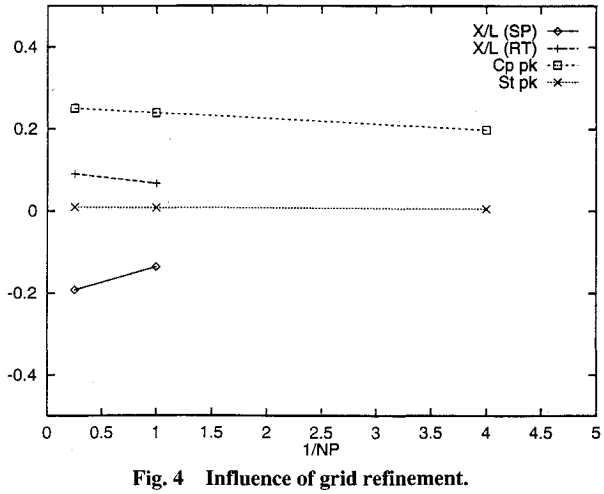

Fig. 4 Influence of grid refinement.

pect ratio affects the resolution of the leading edge shock (whose effects, however, are limited to about 10% of the plate), the location of the separation and reattachment shocks (and the extent of the separation), and the inviscid pressure jump. Good resolution of the flow up to the recirculation bubble can be obtained with a mesh having an aspect ratio ranging between 1.5 and 700. The computed and analytically evaluated [see Eq. (4)] skin friction distributions are reported in Fig. 7. The figure shows that nearly all the grids were able to recover the boundary-layer-type solution. However, it must be pointed out that the peak heating cannot be well-predicted if one assumes an entirely laminar flow. Indeed, applications of the transition criteria given by Eqs. (12) and (13) indicated that the flow was laminar up to the hinge line. This was mainly due to the strong compression across the separation shock, which acted as a

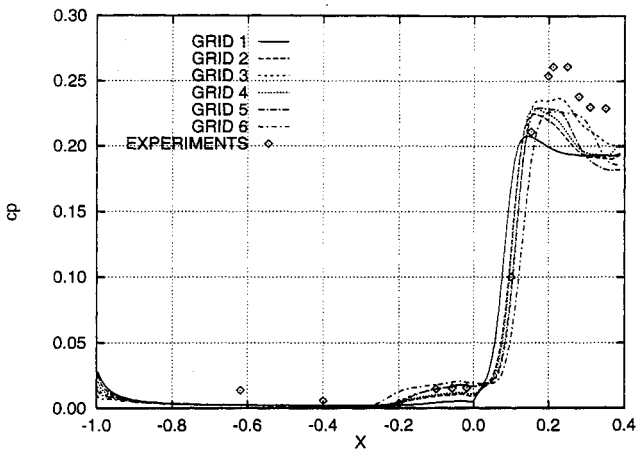

Fig. 5 Test case A: pressure coefficient (laminar computation).

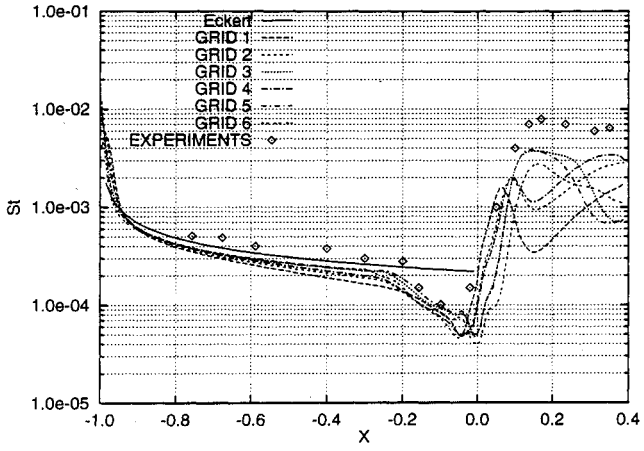

Fig. 6 Test case A: Stanton number (laminar computation).

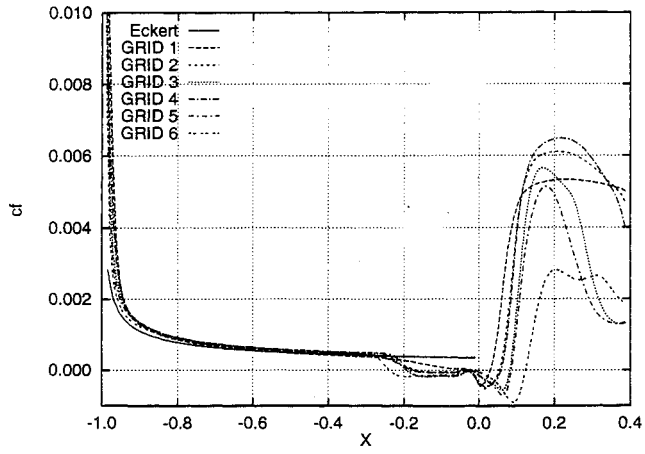

Fig. 7 Test case A: friction coefficient (laminar computation).

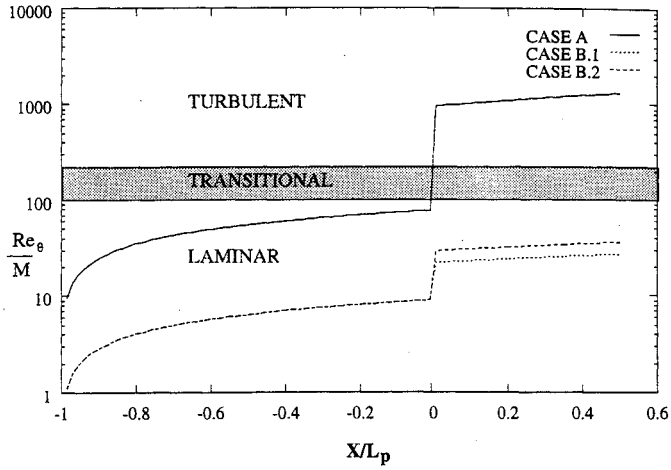

Fig. 8 Transition criteria.

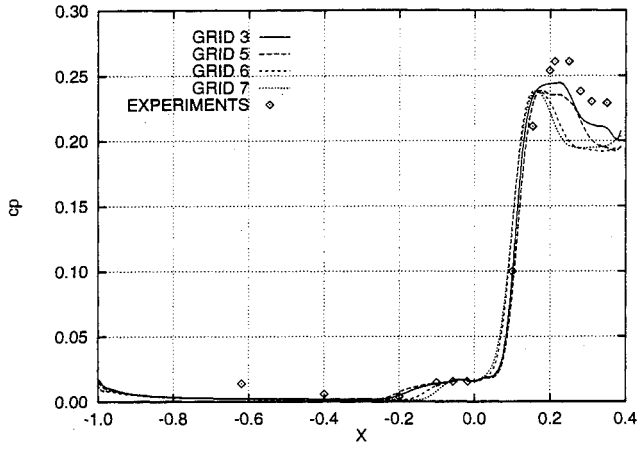

Fig. 9 Test case A: pressure coefficient (turbulent computation).

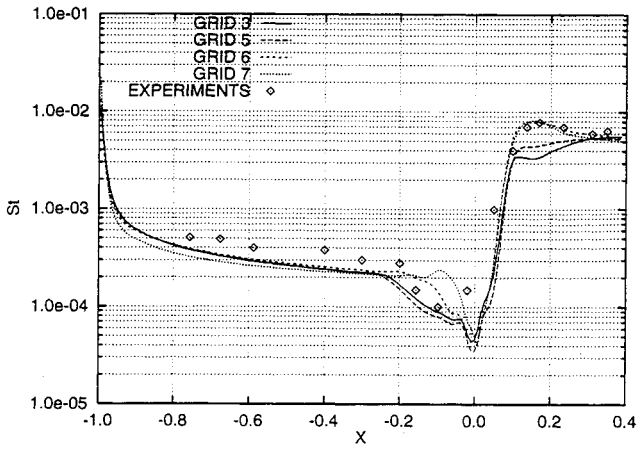

Fig. 10 Test case A: Stanton number (turbulent computation).

disturbance amplifying mechanism.[4] In particular, the transition criteria given by Eq. (13) is reported in Fig. 8, which shows that, for the present test case, the parameter $Re_\theta/M_e \leq \mathcal{O}(10^2)$ up to the hinge line.

Therefore, several computations were performed by assuming laminar flow up to the location where $Re_\theta/M_e \approx \mathcal{O}(200)$, which corresponds to about 5 mm past the hinge, and by assuming fully turbulent flow afterward. With these assumptions made we also used a different grid having a maximum aspect ratio ≈ 2000. The computed pressure and Stanton number distributions are reported in Figs. 9 and 10, which show a dramatic improvement of the resolu-

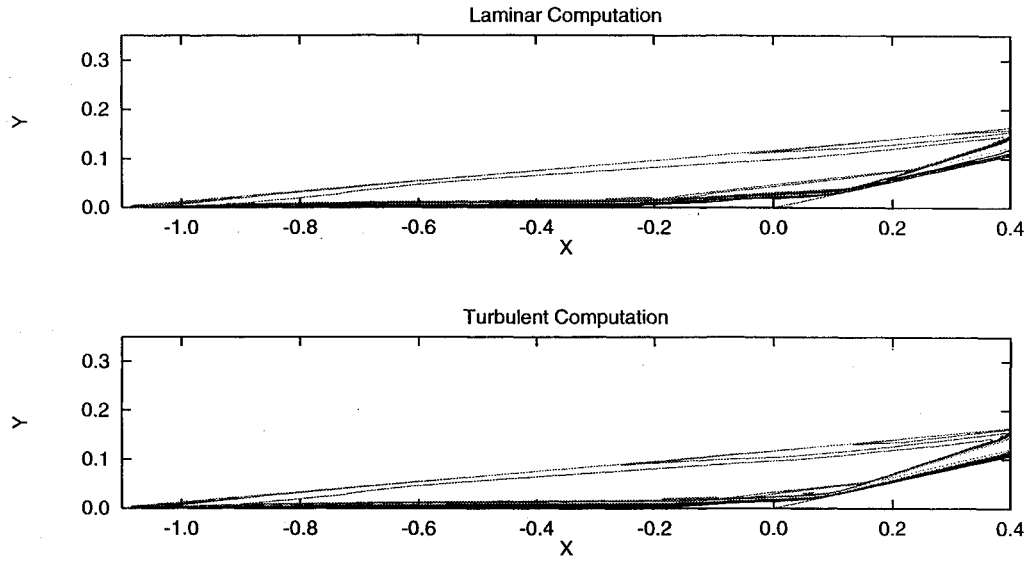

Fig. 11 Test case A: iso-Mach lines (step 0.5).

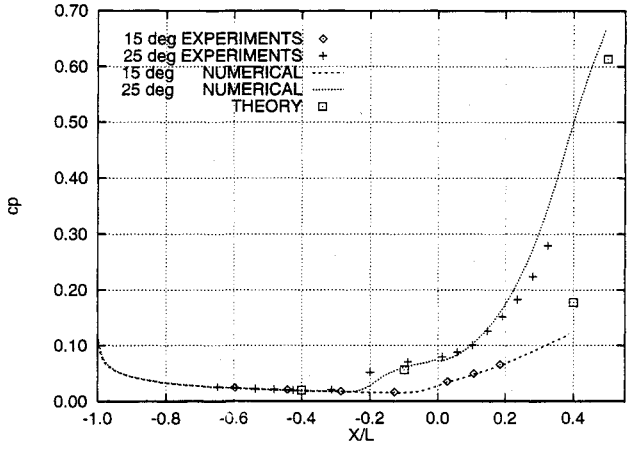

Fig. 12 Test case B: pressure coefficient.

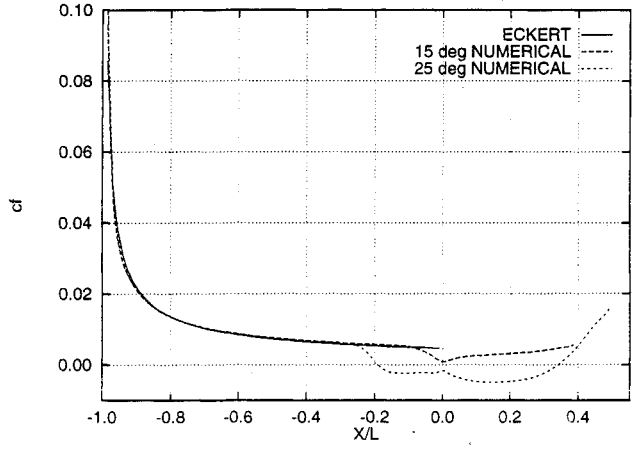

Fig. 13 Test case B: skin friction coefficient.

tion with the correct physical modeling of the flow, and a deterioration of the solution on the last grid due to its excessive stretching, which in turn yielded a poor resolution of the upper part of the recirculation bubble.

The flow details are shown in Fig. 11, where the iso-Mach lines for the fully laminar and the transitional test cases (corresponding to grid 6) are reported. The reduction of the upstream influence when the flow was transitional is clearly evident.

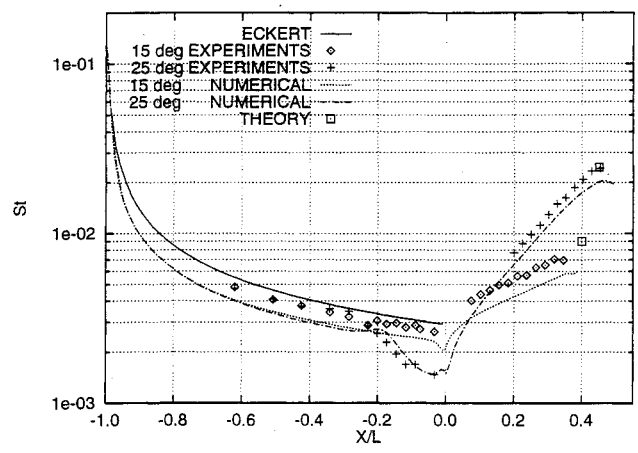

Fig. 14 Test case B: Stanton number.

Test Case B: Laminar Flow

The models used for these experiments also consisted of a two-dimensional flat plate plus ramp configurations. The plate had a sharp leading edge and two ramp angles were considered: $\alpha = 15$ deg and $\alpha = 25$ deg, the total length of the models being equal to 235 mm for $\alpha = 15$ deg and 269 mm for $\alpha = 25$ deg. The length L_p was equal to 179 mm in the two cases, with a span of 150 mm. The experiments were executed at Mach 10 in the hypersonic low-Reynolds-number blow-down wind tunnel of the ONERA Chalais-Meudon Establishment for the following stagnation conditions: pressure of 2.5×10^5 Pa, temperature of 1100 K, yielding a unit Reynolds number equal to 1.65×10^5/m and a molecular mean free path equal to 0.4 mm. These values were intended to insure a laminar flow regime (except in the immediate vicinity of the leading edge). Surface measurements were executed in the model plane of symmetry. Pressures were measured by means of high-sensitivity Validyne transducers placed inside the testing chamber, with care being taken to achieve stabilized conditions through the tubing between the pressure orifices and the transducers. Heat transfer was measured by the thick wall method, the surface temperature being determined by platinum films deposited on a thermally insulated insert.[18] Due to the much lower value of the Reynolds number, the flow over the 15-deg ramp did not separate, with the possible exception of a tiny region at the hinge level. The 25-deg ramp, leading to the formation of an extended separation, was equipped with fences to minimize finite span effects, which otherwise were found to be important.

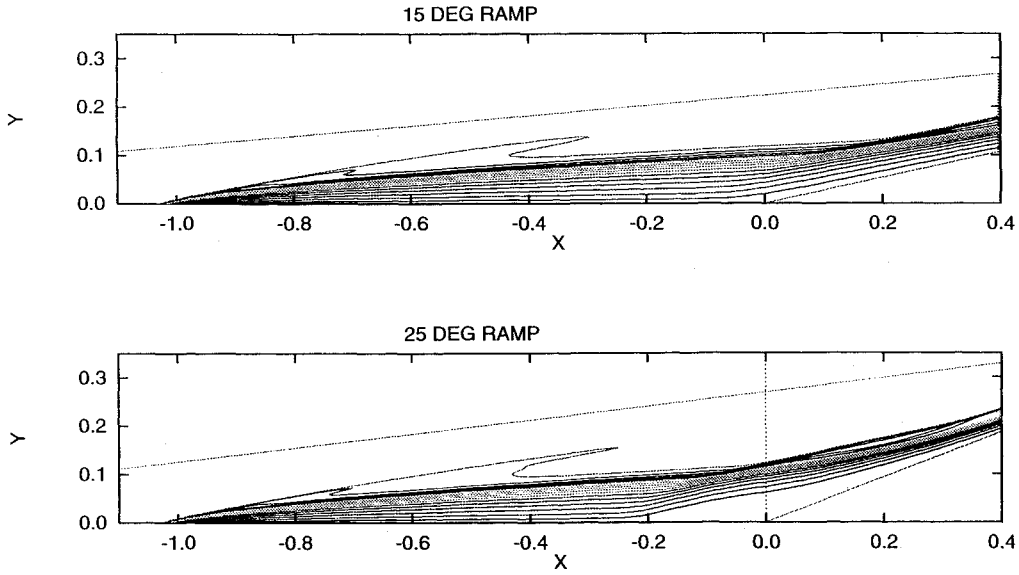

Fig. 15 Test case B: iso-Mach lines (step 0.5).

For this test the Reynolds number was rather low, and the viscous interaction parameter was $\bar{\chi} = 5.4$. As a consequence, the viscous effects played an important role in the establishment of the flow characteristics. Moreover, the application of the transition criteria used before indicated that laminar flow conditions could be assumed throughout as shown in Fig. 8. For the given conditions, Eq. (8) yields an incipient separation angle $\alpha_{is} = 18$ deg. Indeed, both the computed results and the measurements showed an extended separation only for the larger ramp angle. For this test case computations were performed on a 220×64 mesh with a minimum mesh spacing (in the normal direction) approximately equal to 4.5×10^{-2} mm and an aspect ratio ranging between 0.90 and 12 for the 15 deg and 1.70 and 10 for the 25 deg case.

The computed pressure, skin friction, Stanton number distributions, and iso-Mach lines are reported in Figs. 12–15. From the figures we observe that the solutions corresponding to the two ramp angles agreed very well up to the region of the upstream influence, thus confirming the boundary-layer character of the solution along most of the leading edge flat plate. In the case of $\alpha = 25$ deg the flow separated at $x = 4.76$ cm upstream of the corner with reattachment at $x = 7$ cm downstream of the hinge line. The computed pressure and Stanton number distributions show very good agreement with the measured ones, even though some differences in the separation region were observed. Moreover, the computed results show a faster recompression for the 25 deg case. In the figures we have also reported the values of the pressure and the peak heating, evaluated by means of the previously described correlation formulas. The comparison shows that the discrepancies between the computed and analytically evaluated values are of the order of 10%.

V. Conclusions

In the present work we have developed a validation procedure for the analysis of shock-wave/boundary-layer interaction phenomena. However, it must be said that the approach presented here is applicable to different kinds of problems. In particular, we have shown that validation implies both numerical and physical aspects. The former amounts to an assessment of the sensitivity of the solution to the grid (geometry, smoothness, aspect ratio, total number of mesh points, etc.) and to the numerical parameters affecting the numerical solver.

From the computed results we have shown that the aspect ratio of the mesh (primarily through the near wall mesh spacing) affects the leading edge shock resolution and the interaction region. Grid stretching improves the accuracy of the solution in terms of separation, plateau and reattachment pressures, peak heating, etc. However, in the presence of a recirculation bubble an excessive stretching may lead to a deterioration of the resolution in the upper portion of the bubble with a consequent loss in the solution accuracy. Moreover, the streamwise resolution affects primarily the extent of the separation and the location of the separation shock.

The physical aspect of validation requires that experimental and theoretical knowledge of the problem should always be verified to assess the consistency of the computed and experimental solution. In particular, for strong shock-wave/boundary layer interactions we have shown that up to the region of upstream influence the flow recovers the boundary-layer behavior. In the interaction region the flow structure is determined by the separation and reattachment shocks, while the inviscid pressure jump determines the evolution of the flow past reattachment. Hence, a successful simulation requires a careful analysis of the physical problem. Indeed, we have shown that even the use of a simple model may lead to reasonably accurate results. For example, transitional flows can successfully be simulated by using a simple algebraic turbulence model if the latter is coupled with transition criteria.

Acknowledgment

Part of the experimental study has been executed with the financial support of Dassault Aviation in the framework of the HERMES research and development program.

References

[1]Marvin, J. G., "Dryden Lectureship in Research, a Perspective in CFD Validation," AIAA Paper 93-0002, Jan. 1993.

[2]Marvin, J. G., "Accuracy Requirements and Benchmark Experiments for CFD Validation," *Validation of Computational Fluid Dynamics*, Vol. I, AGARD CP437.

[3]Abgrall, R., Desideri, J. A., Glowinski, R., Mallet, M., Periaux, J. (eds.), *Hypersonic Flows for Reentry Problems*, Vol. III, Springer-Verlag, Berlin, 1992.

[4]Grasso, F., and Falconi, D., "On High Speed Turbulence Modeling of Shock-Wave-Boundary Layer Interaction," *AIAA Journal*, Vol. 31, No. 7, 1993, pp. 1199–1206.

[5]Bogdonoff, S. M., "Computational Validation for Hypersonics: An Experimentalist's Perspective," *Workshop on Hypersonic Flows for Reentry Problems* (Antibes, France), Jan. 1993.

[6]Jameson, A., Schmidt, W., and Turkel, E., "Numerical Solutions of the Euler Equations by Finite Volume Methods Using Runge-Kutta Time-Stepping Schemes," AIAA Paper 81-1259, June 1981.

[7]Grasso, F., and Marini, M., "Multigrid Techniques for Viscous Hypersonic Flows," AIAA Paper 93-0771, Jan. 1993.

[8]Baldwin, B. S., and Lomax, H. L., "Thin Layer Approximation and Algebraic Model for Separated Turbulent Flow," AIAA Paper 78-257, Jan. 1978.

[9]Swanson, R. C., and Turkel, E., "On Central Difference and Upwind

Schemes," *Journal of Computational Physics*, Vol. 101, No. 2, Aug. 1992, pp. 292–306.

[10]Eckert, E. R. G., "Engineering Relations for Friction and Heat Transfer to Surfaces in High Velocity Flow," *Journal of Aeronautical Science*, Vol. 23, No. 8, 1956, pp. 585–587.

[11]Delery, J. M., "Shock Interference Phenomena In Hypersonic Flows," Third Joint Europe/US Short Course In Hypersonics (Aachen, Germany), Oct. 1990.

[12]Holden, M. S., "A Study of Flow Separation in Regions of Shock Wave-Boundary Layer Interaction in Hypersonic Flow," AIAA Paper 78-1169, July 1978.

[13]Di Cristina, V., "Three-Dimensional Laminar Boundary Layer Transition on a Sharp 8° Cone at Mach 10," *AIAA Journal*, Vol. 8, No. 5, 1970, pp. 852–856.

[14]Hung, F. T., and Barnett, D. O., "Shock Wave/Boundary Layer Interference Heating Analysis," AIAA Paper 72-237, Jan. 1973.

[15]Chapman, D. R., Kuehn, D. M., and Larson, H., "Investigation of Separated Flows in Supersonic and Subsonic Streams with Emphasis on the Effects of Transition," NACA TN-3869, 1957.

[16]Grasso, F., and Leone, G., "Chemistry Effects in Shock Wave Boundary Layer Interaction Problems," International Union of Theoretical and Applied Mechanics, IUTAM Symposium on Aerothermochemistry of Spacecraft and Associated Hypersonic Flows (Marseille, France), Sept. 1992.

[17]Coet, M. C., Chanetz, B., and Delery, J. M., "Experiments on Shock Wave-Boundary Layer Interaction at High Mach Number with Entropy Layer Effects," International Union of Theoretical and Applied Mechanics," IUTAM Symposium on Aerothermochemistry of Spacecraft and Associated Hypersonic Flows (Marseille, France), Sept. 1992.

[18]Chanetz, B., Coet, M. C., Nicout, D., and Pot, D., "Interaction Onde de choc-Couche limite en Ecoulement Hypersonique Laminaire Bidimensionel (Shock Wave-Boundary Layer Interaction in Hypersonic Two Dimensional Laminar Flow)," Colloque sur les Ecoulements Hypersoniques (Garohy, France), Oct. 1992.